Field-ionization electron detector at low temperature of 10 mK range

AUTHOR(S):

Shibata, M; Tada, M; Kishimoto, Y; Kominato, K; Haseyama, T; Ogawa, I; Matsuki, S; Yamada, S; Funahashi, H; Yamamoto, K

CITATION:

Shibata, M ...[et al]. Field-ionization electron detector at low temperature of 10 mK range. REVIEW OF SCIENTIFIC INSTRUMENTS 2003, 74(7): 3317-3323

ISSUE DATE:

2003-07

URL:

http://hdl.handle.net/2433/39807

REVIEW OF SCIENTIFIC INSTRUMENTS VOLUME 74, NUMBER 7 JULY 2003

Field-ionization electron detector at low temperature of 10 mK range

M. Shibata, M. Tada, Y. Kishimoto,[a] K. Kominato, T. Haseyama, I. Ogawa,[b] and S. Matsuki[c]
Nuclear Science Division, Institute for Chemical Research, Kyoto University, Gokasho, Uji, Kyoto 611-0011, Japan

S. Yamada and H. Funahashi
Department of Physics, Kyoto University, Kyoto 606-8503, Japan

K. Yamamoto
Department of Nuclear Engineering, Kyoto University, Kyoto 606-8501, Japan

(Received 25 February 2003; accepted 1 April 2003)

Selective field-ionization electron detector at low temperature of 10 mK range was developed with a channel electron multiplier. The field-ionization electrode system is attached to the bottom plate of the mixing chamber of a dilution refrigerator and ionized electrons are transported to a channel electron multiplier at the 1 K temperature pumping stage through a series of ring focusing electrodes. The channel electron multiplier is heated up to more than 20 K with a heating coil to maintain its long-term operational conditions, while keeping its environment temperature to 1 K. Rydberg states in Rb with $80 \lesssim n \lesssim 150$ were successfully field ionized and detected with this system at the long-term operating temperature of 12–15 mK. © *2003 American Institute of Physics.*
[DOI: 10.1063/1.1582392]

I. INTRODUCTION

Rydberg atoms have been utilized in many research fields including cavity quantum electrodynamics[1] along with their own physics research.[2,3] In this research, selective field ionization (SFI) is the most commonly used method to detect selectively the Rydberg states,[2,3] in which channel electron multipliers (CEMs) have been usually adopted for detecting the ionized electrons and/or ions.

For these applications Rydberg atoms have been mostly produced and utilized at room temperature. Although a more complex experimental system is required, utilization of Rydberg atoms at lower temperature less than 4 K have interesting potentials for their applications to fundamental physics research as shown in later example.[4] However, usual CEM detectors lose high multiplication gain at lower temperature less than 20–50 K due to increasing resistance between the top and end electrodes, thus preventing the detectors from being used directly at extreme low temperature near to the 10 mK range.

Extending the applications of Rydberg atoms to such extreme low-temperature environment, it is therefore essential to develop field ionization detectors still useful at such low temperature. Here we have developed a quite efficient field-ionization electron detector system with a CEM which can be used even at low temperatures in the 10 mK range.

This development was originally motivated to apply this detector to search for dark matter axions with the Rydberg-atom cavity detector at low temperature.[4] One of the most efficient ways to search for dark matter axions is to convert an axion into a single photon via the Primakoff process in the strong magnetic field with a high-Q microwave cavity. The axion-converted photons in the resonant cavity are absorbed by Rydberg atoms which are exclusively prepared to a lower state and the transition frequency to which some upper state is approximately set equal to the cavity resonant frequency. The Rydberg atoms excited to the upper state are then selectively field ionized and detected with a CEM. In this scheme, noise of the detection system and thus the ultimate sensitivity is almost determined by the background from thermal blackbody radiations in the cavity.[5] It is therefore essential to operate this Rydberg-atom axion detector at a temperature as low as possible.

In this article, design principle and the actual apparatus of the field-ionization electron detector useful at low temperature are described and the characteristics and the performance of the system are presented and discussed. Although the development of the present detector system has been specifically motivated by the above mentioned purpose, the detector can be utilized for more general purposes.

II. DESIGN PRINCIPLE

A. Overview

Essential requirements for the field ionization electron detector at low temperature in the 10 mK range are as follows: (1) the selective field-ionization electrode system has to be located at the mixing chamber plate in order for the Rydberg atoms and the relevant cavity system to be mostly cooled down so that the Rydberg-atom cavity detector works

[a]Present address: Research Center for Neutrino Science, Tohoku University, Sendai 980-8578, Japan.
[b]Present address: Department of Physics, Osaka University, Toyonaka, Osaka 560-0043, Japan.
[c]Author to whom correspondence should be addressed; electronic mail: matsuki@carrack.kuicr.kyoto-u.ac.jp

well under the best condition by keeping its intrinsically low noise character; (2) since the electron multiplier exhausts a resistive power and heats up the environment, it has to be placed somewhere other than the mostly cooled mixing chamber region; and (3) the CEM should be heated to more than 20 K so that it works properly for long running conditions.

In order to fulfill these requirements, a CEM electron detector is located at the 1 K pumping stage and the electrons produced by the field ionization process are transported to the detector through a series of ring focusing electrodes. The CEM detector is heated to more than 20 K with a resistive coil surrounding it, while keeping the temperature of the surrounding port at 1 K.

In addition to the above fundamental requirements, the following features inherent in the present detector system have to be taken into account: (1) since the Rydberg atomic beam is distributed in a rather large cross section ($\sim$6 mm diameter) at the field ionization region to get an enough intensity, field-ionized electrons are also liberated at large volume in the ionization electrodes; (2) the electrons thus have a velocity broadening resulting from the different acceleration between the two electrodes which depends on the ionizing positions; and (3) finally from these characteristics, the electron trajectories cannot be limited to the small region near the central axis, but are rather broadly distributed (nonparaxial beam) within the available space in the transportation through the ring electrodes to get the maximum transport efficiency.

B. Electron transport

Since the available space to install this system is quite limited, the transport electrodes should be as small as possible. We decided to use a series of electrostatic lenses with thin ring electrodes for focusing and transporting the ionized electrons to the detector. All the lenses and the available transport region are covered with superconducting niobium boxes and tubes to expel out the magnetic field of 0.05–0.09 T which is produced by a main superconducting coil and partly reduced with a cancellation coil.[4] The magnetic field is inevitably applied to the cavity for the axion conversion from the present purpose of our axion detector system.[4]

From these inherent characteristics, and also from the circumstances where the focusing electrodes are surrounded by a box and tubes of niobium with grounded potentials, it is more convenient and flexible to do the numerical simulation analyses in three dimensions for designing the electron transport rather than to rely on some analytical calculations. We have decided therefore to use the three-dimensional ion trajectory code SIMION-3D[6] from the beginning of our design study.

Typical focusing property of an electrostatic lens with a thin ring electrode obtained from the simulation calculations is shown in Fig. 1, where the electrons initially in the parallel beam are focused on an electric field of a ring electrode. Here the inner diameter and the thickness along the beam axis of the ring are 15 and 2 mm, respectively. The applied potential to the electrode is 1.5 kV and the electron energy is

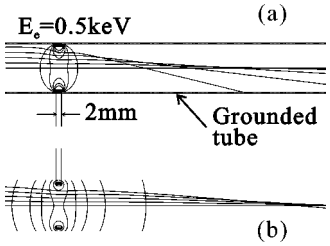

FIG. 1. Typical focusing properties of a ring electrode (a) with and (b) without grounded tubes surrounding it.

0.5 keV. The grounded tube surrounding the ring strongly affects the focusing behavior as clearly seen in the comparison to the case without the tube in Fig. 1. Actually the focal length is not a constant but varies with the beam distance from the central axis in the case of the grounded-potential tube included.

The focal length is also dependent on the thickness and the inner diameter of the ring electrode, in addition to its potential, or the applied voltage. Dependence of the focal length on these parameters was carefully studied with the program SIMION-3D[6] and optimum geometry of the lens system was thus determined.

C. Limitations

The present SFI electrodes were designed to meet the general requirement for both the dc field and the pulsed field ionization schemes.[2,3] This SFI and transport system generally have a limited detection efficiency applicable to some region of SFI voltage. This is due to the fact that since the initial energy of electrons liberated from the field-ionization process varies strongly with the applied voltage at the SFI region, the first electrode potential ($E1$) has to be more increased with increasing SFI electric field (thus with lowering the excitation energy of Rydberg states, or with decreasing the principal quantum number n of Rydberg atoms) to properly transport the electrons.

From our original purpose, the detector system was designed to have a good detection efficiency in the SFI electric field region from 0 to 20 V/cm with which the Rydberg atoms with the principal quantum number n larger than $\sim$80 can be detected. In the present design, the same focusing potentials can be applied for this region of Rydberg atoms. It is noted, however, that it is easy to extend the system for the lower n region, that is for the higher SFI electric field region, by increasing the first $E1$ potential properly.

III. APPARATUS

A. Field-ionization electrodes

Since larger space is required for the ions to be bent with an electric field because of its large momentum, the ionized electrons are guided and detected in the present system. A cross sectional view of the overall structure of the field-ionization electrodes and the adjacent transport system are shown in Fig. 2. An enlarged portion of the ionization electrodes and the following electron transport region up to the first electrode are shown in Figs. 3 (cross-sectional view cut

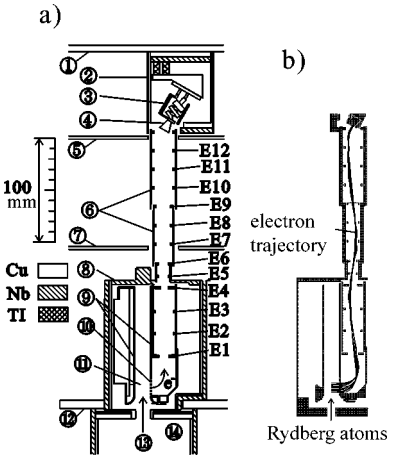

FIG. 2. (a) Cross sectional view of the selective field-ionization system developed especially for the low-temperature environment of 10 mK range and (b) typical electron trajectories from the field-ionization part to the channel electron multiplier. (a) (1) plate for the 1 K pot pumping stage, (2) housing box of Nb for the CEM, (3) a nichrome coil for heating up the CEM to more than 20 K, (4) channel electron multiplier (CEM), (5) plate at the still, (6) Nb tube, (7) plate at the heat-exchanger, called cold plate (C/P), (8) housing box of Nb, (9) electrodes for the field ionization, (10) copper mesh grid to pass the electrons to the transportation region, (11) field-ionization region, (12) plate for the mixing chamber, (13) Rydberg atomic beam, and (14) detection cavity made of copper coated with Nb. TI noted in the figure is Toray TI polymer (Ref. 8). $E1-E12$ represents the ring electrodes (except for the first electrode $E1$ which is of rectangular shape with a central hole) for the transportation of the ionized electrons. (b) Here only the trajectories of electrons liberated from a limited region are shown for avoiding the complexity.

at the same plane as in Fig. 2) and 4 (cross-sectional view cut perpendicular to the plane of Fig. 3). A perspective view of the present field-ionization system is shown in Fig. 5.

The field-ionization electrode system consists of two parallel copper plates 15 mm apart which are widened at one edge near the beam outlet hole from the cavity. The shape of the widening of the two electrodes at the edge was determined in such a way that the electric field along the Rydberg atomic beam path rises up monotonously from the outlet of the cavity and reaches a flat value just before a fine-mesh

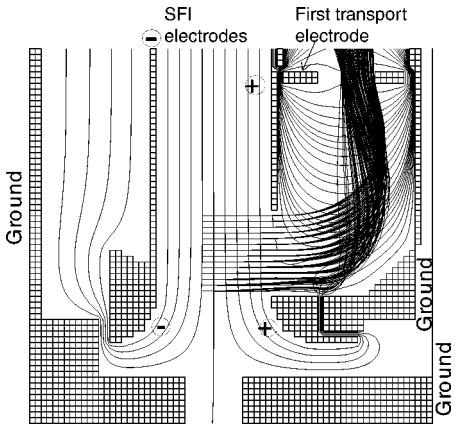

FIG. 3. Cross sectional view of the portion of the selective field-ionization electrodes and the first focusing electrode for electron transportation of the present system. Represented plane is the same as that in the overall system shown in Fig. 2. Equipotential lines at the field-ionization and transportation regions, and some of the simulation results on the electron trajectories are shown with solid lines.

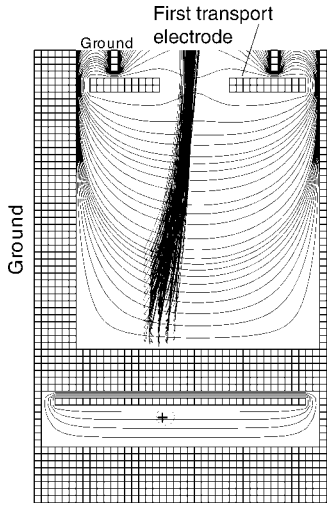

FIG. 4. Cross sectional view of the portion of the selective field-ionization electrodes and the first focusing electrode for the present electron transport system. Represented plane is vertical to that shown in Fig. 3 and includes the central axis of the first focusing electrode. Equipotential lines at the field-ionization and transport regions, and some of the simulation results on the electron trajectories are shown with solid lines.

grid to transport the ionized electrons. A separation distance of 15 mm between the electrode plates was adopted from the requirement that the stray electric field along the Rydberg atomic beam path is small enough to make the selection of the relevant energy states (lower and upper states to be selectively field ionized) possible in the pulsed field-ionization method.[5,7] The stray field actually observed is typically less than 5 mV/cm.

The mesh grid has an area of $15\times15\ \mathrm{mm}^2$, which was incorporated into one of the electrode plates. The equipotential lines at the field-ionization region and at the initial transportation region are shown in Figs. 3 and 4. Uniformity of the electric field at the ionization region, which is approxi-

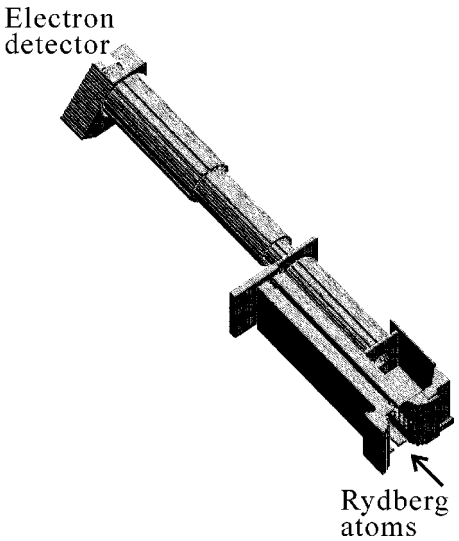

FIG. 5. Perspective view of the present selective field-ionization system for the low-temperature environment of 10 mK range. The field-ionization electrode system is attached to the bottom plate of a mixing chamber, while a channel electron detector is located at the 1 K pot pumping stage. Ionized electrons are transported to the electron detector in the niobium tubes through the 12 focusing electrodes.

TABLE I. Characteristic dimensions and applied voltages of the focusing electrodes $E1-E12$ (rings except for the first one which is of rectangular shape with a central hole): inner hole diameter (i.d.), outer diameter (o.d.), or height×width ($\ell\times\ell$), applied voltage (V), and the position set at the plate of the dilution refrigerator system (place). Thicknesses of all the electrodes along the beam axis are 2 mm.

Electrode E	i.d. (mm)	o.d.($\ell\times\ell$) (mm)	V (kV)[a]	Place
$E1$	10	31×21	0.15	Mx[b]
$E2-3$	18	20	1.0	Mx
$E4$	8	19	1.0	Mx
$E5-6$	10	12	1.0	Mx
$E7-9$	14	16	1.0	c/p[c]
$E10-12$	18	20	1.0	St[d]

[a]Typical values.
[b]Mixing chamber.
[c]Heat exchanger.
[d]Still.

mately equal to the region of mesh grid for the axis along the atomic beam line, is better than 3×10^{-2}.

The Rb atoms, remaining in the ground state without being excited by lasers, are stopped at the 1 K pot plate after leaving the cavity and the field-ionization region. The ions produced by the field-ionization process are also mostly stopped at the same place but some of them are stuck to the wall of the electrodes.

B. Electron transport

Electrons produced by the field-ionization process are transported to CEM at the 1 K pot plate which is about 30 cm apart from the ionization portion. Due to the limited available space in the dilution refrigerator system, the ionized electrons have to be bent 90° after being passed through the mesh grid. The final direction of the ionized electrons is thus vertical and parallel to the direction of the incoming Rydberg atomic beam as seen in Figs. 2–4.

The transport region is divided into four parts, each of which is placed in a box or a tube made of Nb metal to expel out the external magnetic field as shown in Fig. 2. The uppermost and the next upper parts are at 1 K and about 100 mK, respectively, while the lower two parts are attached to the dilution refrigerator section, the temperature being in the 10 mK region.

In total 12 electrodes $E1-E12$ were incorporated along the electron path. The first electrode $E1$ is of rectangular shape with a central hole of 10 mm diameter to transport the electrons, which is contained in a Nb box attached to the bottom plate of the mixing chamber. The following electrodes $E2-E12$ are all of ring shape contained in Nb tubes. The inner diameters, the thicknesses along the beam axis, and the applied potentials of all the electrodes are tabulated in Table I. Typical voltages applied to the first electrode $E1$ and the following electrodes $E2-E12$ are 0.15 and 1.0 kV (the same voltage applied), respectively.

The cross sectional view of an electron ring, its associated Teflon spacer to isolate the electrode from the ground, and a wire lead to connect the electrode to the power supply is shown in Fig. 6. It is noted that the dielectric materials cannot be taken into account in the present version of the

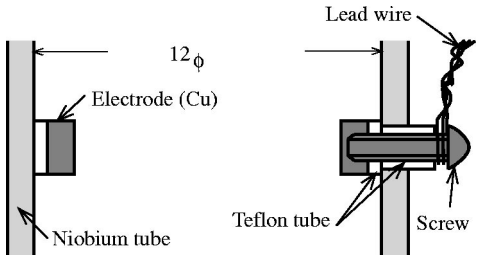

FIG. 6. Cross sectional view of a ring electrode and its associated Teflon rings to support the electrode and isolate it from the ground potential. Since the effect of the dielectric materials on the performance of the electron transportation is quite large, the Teflon rings are kept as small as possible.

SIMION-3D program so that we have to carefully estimate or evaluate the effect of dielectric materials independently of the simulation results with SIMION-3D. In fact we intentionally constructed the transport system in which the inner walls of the Nb rings are all covered with Teflon sheets of 0.5–1 mm thickness to study the effects of the dielectric materials. As shown in the next section, the effect is quite large so that the Teflon spacer was actually designed to have its volume as small as possible to minimize its effect on the performance of the transportation.

Typical electron trajectories in the transportation obtained with the SIMION-3D program are shown in Figs. 2–4 where only some portion of electrons ionized in a limited region of volume at the field-ionization electrodes are shown for avoiding the complexity.

C. Channel electron multiplier

A channel electron multiplier of Burle model 4869 was used for the electron detector. The detector is placed in a niobium housing which is supported with two dielectric rods made of Toray TI polymer[8] from the plate of 1 K pumping stage of the dilution refrigerator system as seen in Fig. 2. This supporting mechanism was adopted to keep the temperature of the 1 K pumping stage low enough to be able to function as originally expected, while the temperature of the CEM is kept higher than 20 K to maintain its performance. In order to keep its temperature higher than 20 K, the CEM is heated up with a nichrome wire surrounding it, in which the dissipation power is about 30 mW. The total dissipation power for the CEM is about 45 mW, including its own self-dissipation due to the applied high voltage.

IV. PERFORMANCE AND DISCUSSION

A. Excitation and detection of Rydberg states

Field ionization characteristics were measured with the Rb Rydberg atoms at the $80\lesssim n\lesssim150$ region. Rydberg atoms in a beam were produced just before entering into the cavity by a two-step laser-excitation scheme from the $5s_{1/2}$ ground state through the $5p_{3/2}$ second excited state.[5,7] Typical excitation spectrum of Rb Rydberg states near $111s-112s$ is shown in Fig. 7, where the ionized electrons were detected by applying a linearly ramped pulse to the electrodes. Here in order to appreciably excite the manifold states and p

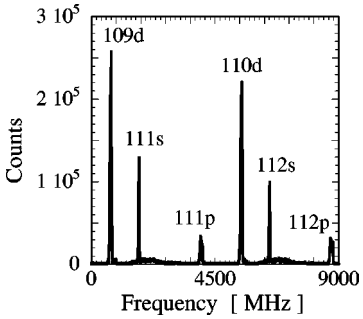

FIG. 7. Typical excitation spectrum of Rb Rydberg states around $111s-112s$. The abscissa represents the frequency of the second laser in relative units. In order to excite the manifold states appreciably, a static electric field of 79 mV/cm was applied to the laser excitation point in the electrodes.

states, a small electric field (79 mV/cm) was applied to the region of laser excitation. The spectrum was measured by varying the wavelength of the second laser.

A typical field-ionization electron spectrum observed by applying a linearly ramped electric field is shown in Fig. 8, where the $111p$ Rydberg state in Rb was initially excited and subsequently field ionized and detected. The electron signals were fed to the timing analyzer (FastComTec P7886) in which the time difference between the start of the linearly ramped field pulse and the electron signals was measured. This raw timing spectrum was then converted to that for the applied electric field strength. We observed that two peaks in the spectrum are due to two different processes in the pulsed field ionization in alkali atoms as revealed in our investigations.[5,7] Present results shown in Fig. 8 were taken with the method of *backward* driving[5,7] in the pulsed field-ionization scheme.

Stringent selectivity in SFI is obtained with a pulsed electric-field-ionization scheme: By applying the properly shaped pulsed electric field, it is possible to manipulate ionization paths in a Stark level structure, resulting in quite stringent selectivity in the field-ionization detection of highly excited Rydberg atoms.[5,7]

B. Characteristics of the electron transport system

Transport efficiency of the present electron detector system was measured at room temperature with a separate setup

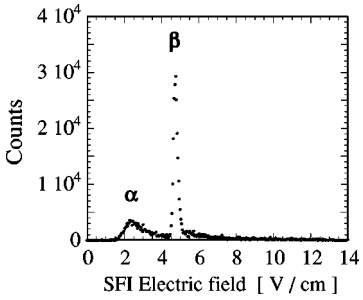

FIG. 8. Typical spectrum of electrons detected with the present field-ionization (SFI) detector at low temperature. The $111p$ state of Rb was ionized by applying a linearly ramped electric field pulse to the field-ionization electrodes. The lower (α) and upper (β) peaks are due to the autoionization-like and tunneling processes, respectively. See Refs. 5 and 7 for the characteristics of the relevant pulsed field-ionization processes.

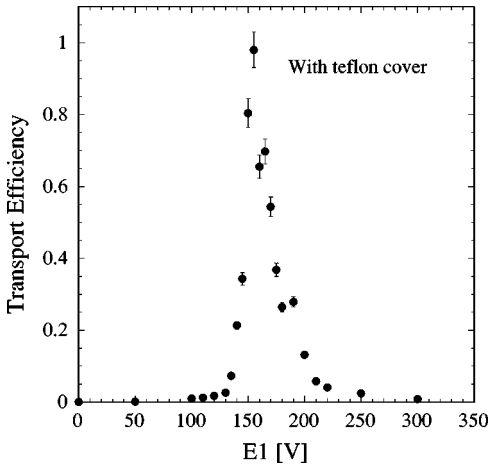

FIG. 9. Absolute transport efficiency of an intentionally built transport system in which all the inner walls of the transport Nb tubes were intentionally covered with Teflon sheets to study the effect of dielectric materials in the transport area. The applied $E2-E12$ voltage and the SFI field are 1.0 kV and 4.7 V/cm, respectively. This measurement was made by using the same setup as the present system without Teflon sheets.

of the experimental system, where another CEM detector was placed as a reference at the opposite side to the present electron transport system, both facing a single field-ionization electrode system. To properly compare the electron counts from both CEM, the signal events from each CEM were counted by switching the applied potential to the electrodes periodically from positive to negative and vice versa each 5 s, thus allowing us to count the number of electron signals from both CEMs without any appreciable effect of the time variation in the experimental system such as Rydberg atomic beam and lasers. The $111s$ state of Rb was initially excited and field ionized for this measurement.

It is noted here that the absolute electron-detection efficiency of each CEM detector has its own characteristic value[9] so that the measured counts from each detector have to be corrected for their absolute efficiencies. The correction factor for this difference was obtained from a direct comparison of the counts from each detector with another different setup, in which the two CEM detectors were set symmetrically to the opposite side of a single pair of ionization electrodes without any transport system. The correction factor, which comes from the difference of the absolute detection efficiency between the two CEMs, was found to be 0.85 ± 0.05 (15% difference in their detection efficiency). All the results described below were thus corrected by this factor.

As noted in the previous section, we first studied the effect of Teflon spacer on the electron transport characteristics. Figure 9 shows the electron transport efficiency of a test system in which the inner walls of all the Nb tubes were covered with thin Teflon sheets (thickness is 0.5–1.0 mm) for the isolation. The observed efficiency strongly depends on the applied $E1$ voltage, while the simulation results without taking into account the effect of Teflon (not shown here) predicts almost flat dependence on the $E1$ voltage. From this observation, we made the Teflon spacer as small as possible between the copper ring and the Nb tube as shown in the previous section.

Figure 10 shows the dependence of the absolute trans-

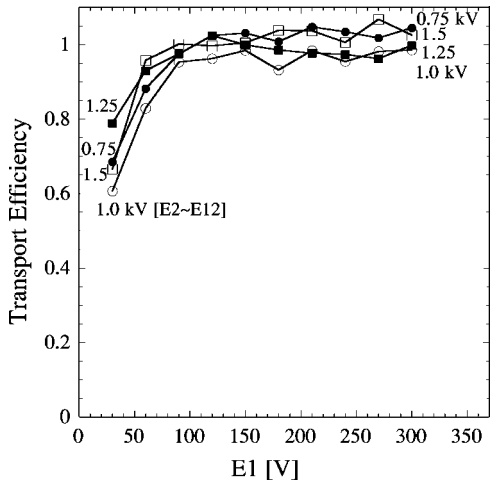

FIG. 10. Dependence of the absolute transport efficiencies of the present detector system on the potential of the first electrode $E1$ and of the following electrodes $E2-E12$. The ordinate shows the ratio of the electron counts detected by the present transport system to that from the reference CEM which was set directly to the opposite side of the field-ionization electrodes without any transport system. The ratio was corrected for the difference (15%) of the absolute detection efficiencies between the two CEM used. Lines drawn are to guide the eye and errors of the data are typically 5%. This measurement was made by using a separate experimental setup apart from the low-temperature cryostat system.

port efficiency of the present system on the applied potential of the first electrode $E1$ and of the following electrodes $E2-E12$, where the ratio of the counts from the present transport system to that from the reference CEM was measured as functions of $E1$ and $E2-E12$. The SFI field dependence of the transport efficiency is also shown in Fig. 11, where the voltages applied to $E1$ and $E2-E12$ are 150 V and 1.0 kV, respectively.

The experimental results on the $E1$ and $E2-E12$ dependence of the transport efficiency show flat distributions at the region of $E1 \geqslant 100$ V and of $E2-E12 \geqslant 0.75$ kV, where the absolute transport efficiencies measured are $100\% \pm 5\%$.

Transport efficiency for the ionized electrons produced at the region in the field-ionization electrodes was thus determined to be $98\%+2\%, -3\%$, in which the electron loss of 2% is included, because a mesh grid is inserted near electrode $E9$ to eliminate the external microwave radiations from

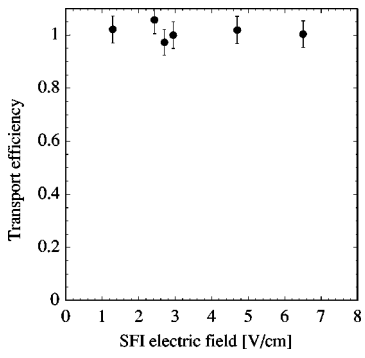

FIG. 11. Dependence of the absolute transport efficiency of the present electron transport system on the electric field for the selective field ionization. Here the applied potentials to the transport electrodes $E1$ and $E2-E12$ are 150 V and 1.0 kV, respectively. See caption of Fig. 10 for the method of obtaining the transport efficiency.

higher temperature regions into the field-ionization area. This loss of 2% was estimated from the occupied area of mesh wires across the line of the Rydberg atomic beam.

The simulation results (not shown here) are in agreement with the experimental results in that they predict the efficiency of $\sim 100\%$, although the predictions show that the efficiency is somewhat reduced with increasing voltages of $E1$ and $E2-E12$ and also with increasing SFI electric field.

C. Operating conditions and adjacent equipment

After good vacuum condition is achieved for the inner vacuum chamber, the cavity and the detector system begin to cool down, first with liquid nitrogen by filling the He can (main bath) and then with liquid He. During the course of this cooling, the heater of the electron detector remains on to reduce the absorption of cooling gas into the surface of the CEM. This treatment is also useful in keeping the temperature of the CEM high enough to maintain its working condition well, thereby allowing the CEM to work properly at any time after cooling and the following re-evacuations. The detector system works quite well for a long time without any deterioration of its performance.

In order to check the operational condition of the CEM, a small filament of tungsten is always installed near the detector housing. Emitted electrons from the heated filament are utilized for monitoring the CEM. This checking system works also quite well even at the mostly cooled stage. Note, however, that the heating of the filament causes the steep rise of the cavity temperature so that the monitoring should be performed in a short time.

Finally it is noted that the weight of the cavity system is about 25 kg and it takes about 5 h for the whole system to be cooled down to 12–15 mK after the pumping of the ^{3}He/^{4}He mixture gas was started. The temperature at the mixing chamber and the cavity was measured accurately several times with the anisotropy distribution of γ rays from an oriented ^{60}Co single crystal source. In usual operations for experiments, however, a number of resistive thermometers with RuO_2 were used for the temperature measurements at several places on the cavity.

ACKNOWLEDGMENTS

This research was partly supported by a Grant-in-Aid for Specially Promoted Research (Grant No. 09102010) by the Ministry of Education, Science, Sports, and Culture, Japan. M.T., S.Y., and T.H. are thankful for the financial support from the JSPS, Japan under the Research Fellowships for the Young Scientist.

[1] Recent review includes *Cavity Quantum Electrodynamics*, edited by P. Berman (Academic, Boston, MA, 1994); A. Rauschenbeutel *et al.*, Phys. Rev. Lett. **83**, 5166 (1999); J. M. Raimond, M. Brune, and S. Haroche, Rev. Mod. Phys. **73**, 565 (2001).
[2] *Rydberg States of Atoms and Molecules*, edited by R. F. Stebbings and F. B. Dunning (Cambridge University Press, Cambridge, 1983).
[3] T. M. Gallagher, *Rydberg Atoms* (Cambridge University Press, Cambridge, 1994), and references cited therein.
[4] S. Matsuki and K. Yamamoto, Phys. Lett. B **263**, 523 (1991); I. Ogawa, S.

Matsuki, and K. Yamamoto, Phys. Rev. D **53**, R1740 (1996); K. Yamamoto and S. Matsuki, Nucl. Phys. B (Proc. Suppl.) **72**, 132 (1999); M. Tada *et al.*, *ibid.* **72**, 164 (1999).
[5] M. Tada *et al.*, Phys. Lett. A **303**, 285 (2002).
[6] D. A. Dahr, Rep. No. INEEL-95/0403, Rev. 5, 2000; see also URL: http://www.sisweb.com
[7] Y. Kishimoto *et al.*, Phys. Lett. A **303**, 279 (2002).
[8] Toray co. Ltd., URL: http://www.toray.com
[9] M. P. Seah, J. Electron Spectrosc. Relat. Phenom. **50**, 137 (1990); *ibid.* **58**, 345 (1992); M. P. Seah and G. C. Smith, Rev. Sci. Instrum. **62**, 62 (1992); J. A. Sawicki, B. D. Sawicka, and F. E. Wagner, Nucl. Instrum. Methods Phys. Res. B **16**, 253 (1991); P. Henkel and E. Kurz, *Bibliography of Detection Efficiency of CEMs, CEMAs, MEMs, and Other Electron Multipliers* (Galileo Electro-optics Corp., Sturbridge, MA); C. A. Keller and B. H. Cooper, Rev. Sci. Instrum. **67**, 2760 (1996), and references cited therein.